The Karla impact structure (Russia) explored by potential-field investigations

Yoann Quesnel, Natalia S. Bezaeva, Dilyara M. Kuzina, Pierre Rochette, Jérôme Gattacceca, Minoru Uehara, Dmitry D. Badyukov, Bulat M. Nasyrtdinov, Dmitry A. Chareev, Cedric Champollion

The Meteoritical Society

Meteoritics & Planetary Science 1–15 (2022)
doi: 10.1111/maps.13806

The Karla impact structure (Russia) explored by potential-field investigations

Yoann QUESNEL*[1], Natalia S. BEZAEVA[2], Dilyara M. KUZINA[3], Pierre ROCHETTE[1], Jérôme GATTACCECA[1], Minoru UEHARA[1], Dmitry D. BADYUKOV[2], Bulat M. NASYRTDINOV[3], Dmitry A. CHAREEV[4,5,6], and Cedric CHAMPOLLION[7]

[1]Aix-Marseille Université, CNRS, IRD, INRAE, CEREGE, Aix-en-Provence, France
[2]V.I. Vernadsky Institute of Geochemistry and Analytical Chemistry, Russian Academy of Sciences, 19 Kosygin str, 119991 Moscow, Russia
[3]Institute of Geology and Petroleum Technologies, Kazan Federal University, 4/5 Kremlyovskaya Str, 420008 Kazan, Russia
[4]Institute Experimental Mineralogy, Russian Academy of Science, 4 Academician Osipyan Str, 142432 Chernogolovka, Moscow Region, Russia
[5]Institute of Physics and Technology, Ural Federal University, 19 Mira Str, 620002 Ekaterinburg, Russia
[6]National University of Science and Technology "MISiS," 4 Leninsky Prospekt, 119049 Moscow, Russia
[7]Géosciences Montpellier, CNRS, Université de Montpellier, Montpellier, France
*Corresponding author. E-mail: quesnel@cerege.fr

(Received 29 March 2021; revision accepted 18 February 2022)

Abstract–With no significant topographic expression and limited bedrock exposure, the ~10 km diameter Karla impact structure (Tatarstan, Russia) is poorly known. The age of the impact is also poorly constrained stratigraphically to between 4 and 60 Ma, even if an upper Miocene age is more likely. Targeted gravity and magnetic field surveys were conducted over Karla to explore its size and structure in 2019. Bouguer gravity anomaly data reveal a central positive (+2 mGal) peak ~2 km in diameter surrounded by a concentric negative (−1 mGal) anomaly extending to ~3 km radius; a more irregular, outward-decreasing (+1 to −1 mGal) positive anomaly extends to 6–8 km radius. A complex impact structure with diameter of 8–10 km is consistent with the Bouguer anomalies. Magnetic field data show 1 to several km-wavelength anomalies with amplitude variation from +150 to −150 nT and little concentric structure, although the impact feature broadly corresponds to a magnetic low with a weak central high. A 2-D numerical model of the structure was built using these potential-field data and petrophysical properties measured on collected samples. It confirms a central uplift composed of Paleozoic sediments and Archean crystalline basement up to 1 km of depth. A 500 m deep collapsed disruption cavity filled by breccia and lacustrine deposits accounts for the Bouguer negative ring. The reversely polarized and weak central magnetic anomalies are controlled by the geometry of the crystalline basement associated with the deformation during the central uplift.

INTRODUCTION

The 208 proven impact structures on Earth show a wide range of preservation state (Gottwald et al., 2020; Kenkmann, 2021): visible and little eroded (e.g., Barringer, USA), strongly eroded (e.g., Tunnunik, Canada), completely erased with very few remains (e.g., Agoudal, Morocco), entirely buried but still well preserved (e.g., Chicxulub, Mexico), partially buried and/or underwater, etc. Indeed, the fate of impact structures on Earth depends on the regional climatic (erosion and burial) and geodynamic (including tectonic, volcanic, metamorphic activity) conditions, erasing the crater. The preservation of the crater morphology is also linked to the age of the impact event, the size of the crater, the target lithology, and the continental or marine setting. Even geologically young and medium-size (5–50 km diameter) to large (>50 km) impact structures can be completely filled or buried, like Mjolnir (Norway), Chesapeake Bay (USA), or Logoisk (Belarus), while geologically old structures can still show a circular morphology and/or impact breccias like

Manicouagan and Tunnunik (Canada). Moreover, the present-day appearance of some impact structures is enigmatic with regard to their estimated size, like the Rochechouart structure (France), and/or to their age. These uncertainties are linked to the lack of geological and geophysical data acquired over these structures.

The Karla impact structure (Russia) belongs to this category of poorly constrained impact structures (Masaitis et al., 1976, 1980) with no clear topographic expression (Fig. 1). Vegetation, recent alluvions, and scarcity of outcrops largely prevent precise mapping of the structure, even if Masaitis et al. (1980) suggested a 10 km diameter based on the estimated extent of the brecciated formations, as well as on the results of several regional drill holes (Masaitis, 1999). However, these constraints are relatively poor, and the present-day preservation state and extent of the impact structure are still not known. Our study aims at giving new insights about the size and the structure of the eroded Karla impact crater. To reach this objective on an eroded structure that is largely hidden, geophysics must be used, as a complement or alternative to drilling. For a first look inside the impact structure, potential-field investigations are the most rapid and efficient methods. We first present the geological setting and the impactites, before describing the geophysical survey that we conducted to unveil the geometry of the impact structure. Our results are then analyzed and integrated in a forward numerical model which will serve to discuss the size and postimpact history of this poorly studied impact structure.

GEOLOGICAL CONTEXT

Landscape and Target Lithologies

The Karla impact structure (54.95°N, 47.97°E) is located in the East European plain of Russia, about 120 km southwest of Kazan in the Republic of Tatarstan. Its relief does not at all reveal the existence of an impact structure, with an overall relatively flat topography ranging from 100 to 220 m of altitude (Fig. 1), mainly controlled by the E-W valley of the Karla River, which joins the N-S valley of the Sviyaga River to the east. Crop fields are the major components of the landscape, with areas of pine forest in the Karla river valley. Therefore, there is no significant morphological signature of an impact event in this area, except, perhaps, along the NW rim of the expected 10 km diameter crater, which corresponds to a curved

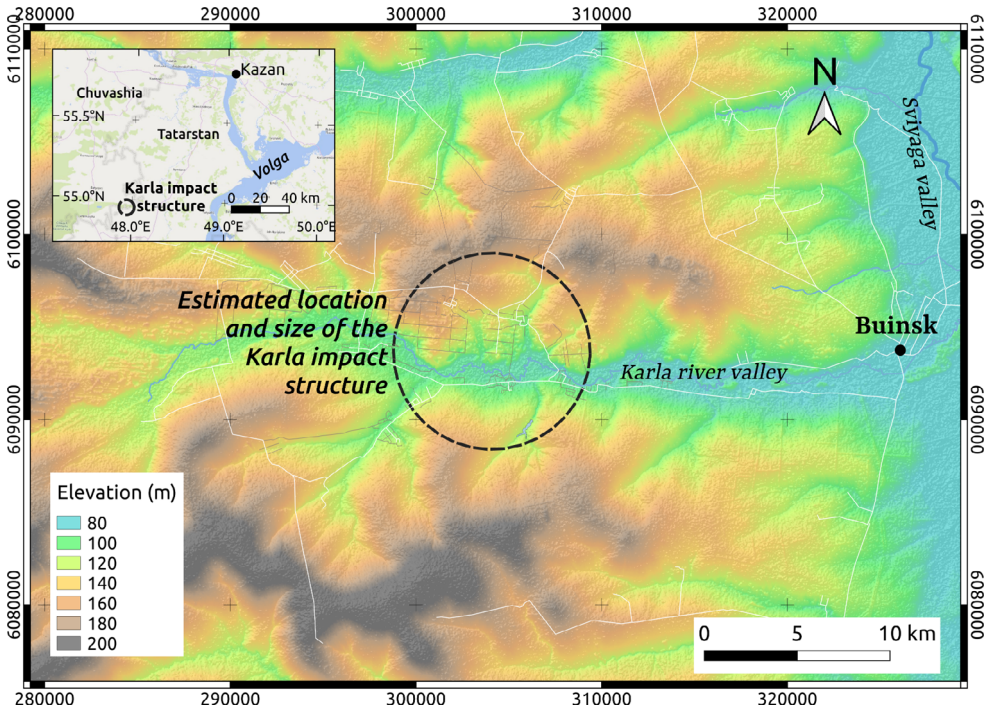

Fig. 1. Topographical map of the Karla impact structure. Inset shows the geographical location of the structure southwest of the city of Kazan. The 30 arc second Shuttle Radar Topography Mission (SRTM) elevation grid was used for elevation. The white lines correspond to the local primary and secondary roads. Coordinates are expressed in meters in the UTM Zone 39U projection with WGS84 datum, except for the inset with geographical coordinates.

topographic high at about 180 m of elevation (Fig. 1). The target rocks consist of a 1.7 km-thick sedimentary sequence with, from bottom to top: about 1200 m of Devonian and Carboniferous limestones and dolomites; 320 m of Permian dolomites, limestones, and terrigenous rocks; 100 m of Jurassic clays and sandstones; and 100 m of Cretaceous clays (Masaitis, 1999). This sequence is locally covered by Neogene and Quaternary deposits, and appears very regular, almost horizontal-lying, at the regional scale (Semakin et al., 1999). Two deep regional drill holes reached the Archaean gneissic basement at about 1.7 km of depth; a series of shallower (300–400 m) drill holes cross the area intersecting the external and impact-disturbed Mesozoic and Permian units. Local rivers, including the Karla, cut the sedimentary layers down to the Permian series before joining the Volga toward the NE. Paleogene and Miocene deposits are missing in the area, due to erosion or because there was no sedimentation due to the progressive uplift of the area (Popov et al., 2006).

The Karla Impact Breccias

The impact structure is characterized by crater fill deposits ("allogenic breccia" of Masaitis et al., 1980; Masaitis, 1999) consisting of mega-blocks (up to 1 km) of middle Carboniferous carbonate rocks up to upper Cretaceous clay inclusions set in a clastic matrix of the same nature, with a maximum thickness of 500 m, according to drilling. This allochthonous breccia formation is described by Semakin et al. (1999) as extending up to 4 km from the center on average (Fig. 2), and locally as far as about 8 km toward N (ejectas?). It is overlain by a thin (15 m maximum observed thickness) distinct layer of fine-grained porous melt-bearing impact breccia containing cm-sized clay and carbonate clasts that was not described previously in the geological map and drill holes (Semakin et al., 1999) or in the general description of the crater (Masaitis, 1999; Masaitis et al., 1980). These formations are covered by Pliocene lacustrine deposits with 100 m of maximum thickness, which sedimented in the lake that filled the trough of the crater (Fig. 2), and ultimately by Quaternary deposits.

The age of the impact is older than early Pliocene because sediments of that age are found at the bottom of the lacustrine sediments filling the crater (Semakin et al., 1999). The older limit for the age is set by the age of the youngest clasts in the underlying allochthonous breccia formation. Clasts made of Miocene "Opoka" formation have been described by Masaitis (1999). It is noteworthy that Opoka formations are marine silica-rich sedimentary rocks that are found in the Cretaceous and Paleogene of Poland and Russia. Paleogeographic reconstructions for the Miocene show that the general area where the Karla impact structure is located was continental (e.g., Popov et al., 2006). Therefore, the description of Miocene Opoka clasts in Masaitis (1999) is highly questionable and must be taken with care. Moreover, Masaitis et al. (1980) had described Opoka clasts of Syzranian age as the youngest clasts in the allochthonous breccia, and proposed an age of 5 ± 1 Ma for the impact, but this is clearly an error since Syzranian correlates with Danian and Selandian in the Paleocene, covering an age range of 59.2–66.0 Ma (Gradstein et al., 2020). Assuming that the Opoka clasts found in the allochthonous breccia are indeed of Syzranian age (Masaitis et al., 1980), the age of the crater would therefore be constrained stratigraphically only between ~4 Ma (age of oldest lacustrine sediments filling the crater) and ~66 Ma (older bound of the Syzranian stage). However, the age of the impact is likely much closer to the younger bound of this interval as there is neither Paleogene nor Miocene sediments in the lacustrine crater fill sequence.

Geological Structure of Karla

The deep structure of Karla is relatively poorly defined. In the allochthonous breccia cropping out in the quarries located close to the center of the structure, Masaitis et al. (1980) observed blocks of Carboniferous rocks, which they interpreted as remains of a central uplift (see also Masaitis, 1999). The contacts between the allochthonous breccia formations and the regional surrounding geology are difficult to characterize, but they are mapped as overthrusting faults mainly striking SW-NE (Semakin et al., 1999). The cross sections interpreted from the drill holes and the partial (because of very few exposures) geological mapping reveal a very disturbed geometry for these allochthonous breccia formations, with slumped or uplifted lenses originating from different stratigraphic layers, with 500–600 m of maximum thickness, and over 10 km of mean lateral extent (Fig. 2) (Semakin et al., 1999). The NW-SE cross section indicates that the Pliocene sediments may have filled the trough around a narrow central uplift. All these data clearly unveil the anomalous geology of this area. It is important to know that the most recent geological mapping and associated cross sections (Fig. 2) were built without interpreting Karla as an impact structure. The leaflet associated with the geological map and cross sections (Semakin et al., 1999) refers to this area as a significant SW-NE shear zone where rocks were damaged by tectonic movements along two regional faults. The central uplift is described as the remains of an accretionary prism, containing "tectonite" rocks. However, the occurrence of shatter

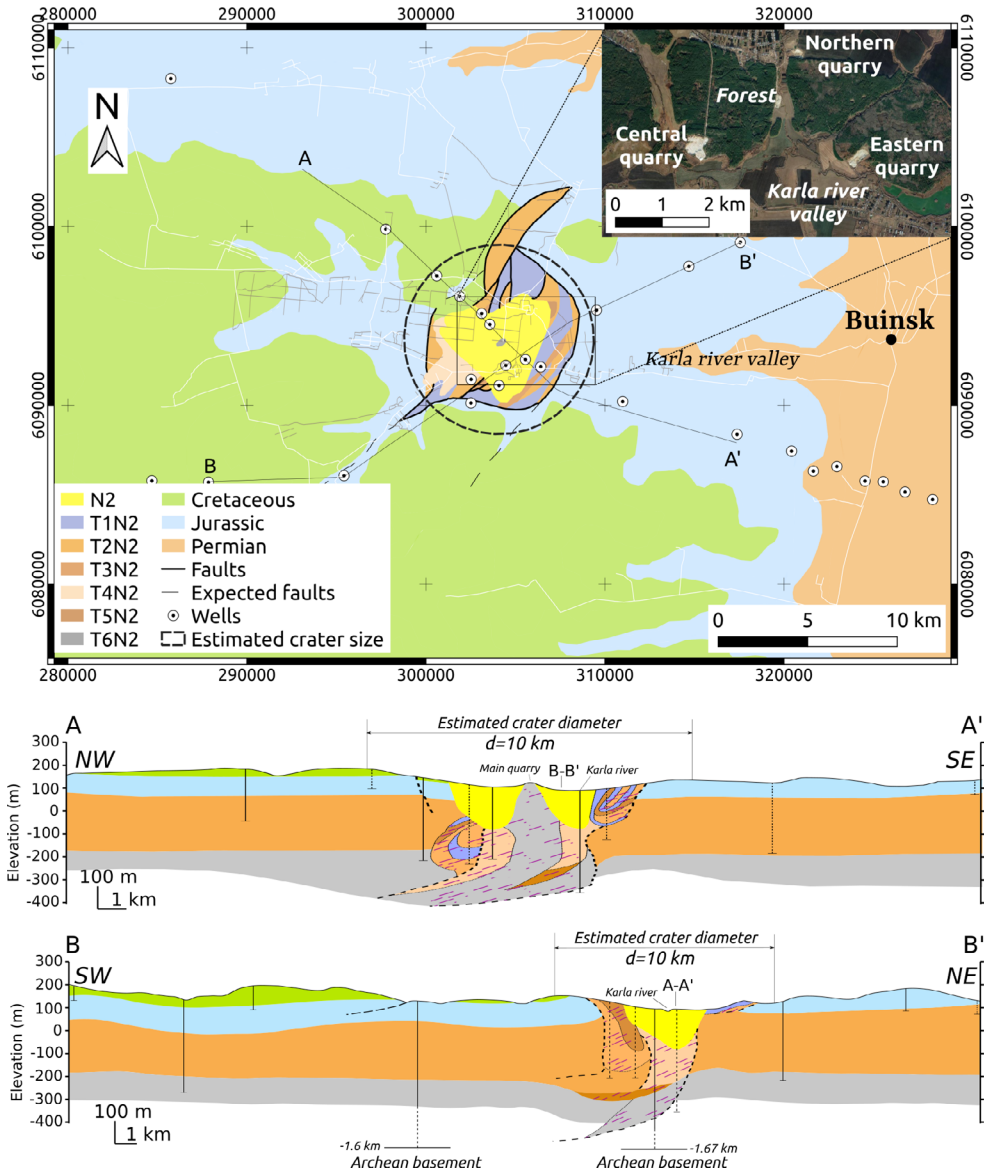

Fig. 2. Geological map (top) and associated cross sections (bottom) of the Karla impact structure. Inset in the geological map corresponds to a Bing satellite view of the central part of the structure, zooming in the quarries. This geological map was slightly modified from the 1:200000 N38-XII and N-39-VII maps produced by Semakin et al. (1999). For clarity, Quaternary and Akchagylian (latest Pliocene to early Pleistocene) deposits are not shown. Lithologies are: N2, pliocene deposits of clays and siltstones; T1N2, brecciated/fractured rocks of Jurassic age; T2N2 and T3N2, brecciated/fractured rocks of upper Permian age (Tatarian and Kazanian stages); T4N2, T5N2, and T6N2, shock-processed bodies of intrusive brecciated rocks of Upper Permian, Lower Permian, and Carboniferous ages (all T1N2 to T6N2 formations belong to the allochthonous breccia described in Masaitis, 1999); Cretaceous, Barremian-Hauterivian stage deposits mainly composed of clays with sand and siltstone lenses; Jurassic, Tithonian, Oxfordian, Kimmeridgian, and Callovian stage deposits of clays and/or marls with sand and siltstone lenses; Permian, Tatarian stage deposits of clays, siltstones, sandstones, and marls. Same UTM Zone 39U coordinate system (in meters) as for Fig. 1. The associated cross sections AA′ and BB′ have a vertical exaggeration of 10. The gray deep formation corresponds to Devonian-Carboniferous limestones and dolomites. Purple hatching highlights brecciated/fractured zones. Drill holes represented with a solid vertical line indicate drillings located along the considered profiles, whereas those with a dashed line correspond to adjacent drillings projected on the profiles.

cones proves that the Karla structure was caused by an impact. Masaitis ([1999] and references within) reported that these shatter cones were collected within and nearby the quarries at the center of the structure (Figs. 1 and 2), and better described the geology by mentioning "allogenic breccia" instead of slumped/

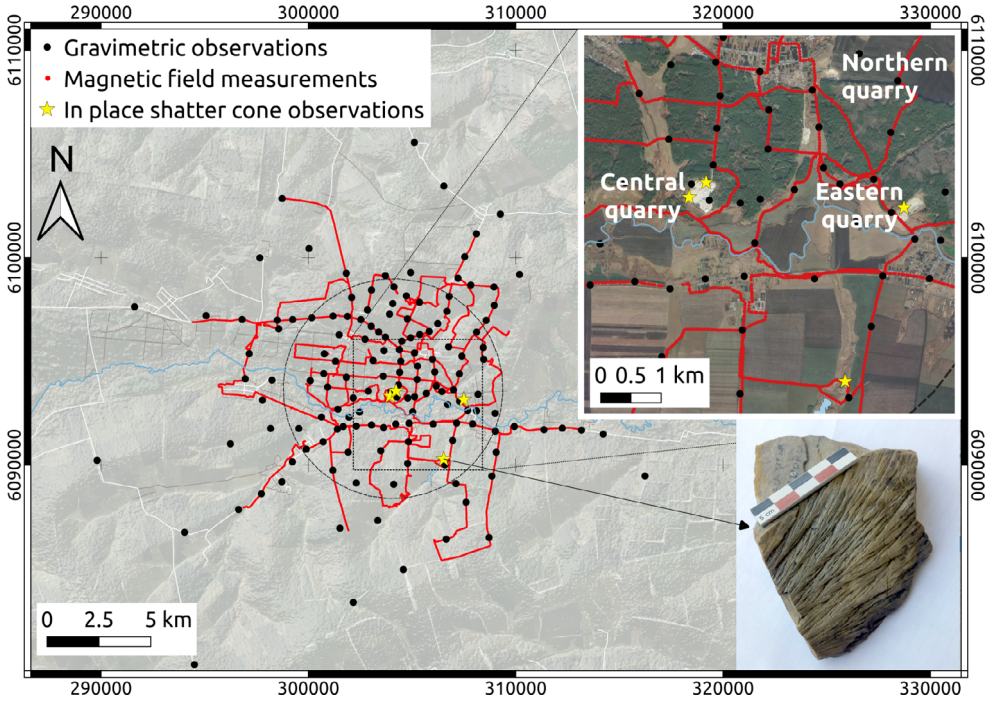

Fig. 3. Location map of ground magnetic field (in red) and gravity (black dots) measurement stations. The top right inset zooms in the central area with the quarries. Yellow stars correspond to sites where in situ shatter cones have been observed (bottom right inset shows one shatter cone sampled about 4 km southeast from the main quarry). The dotted circle is the structure diameter estimated by Masaitis (1999). As for Fig. 1, grayscaled SRTM digital elevation model is used as background and UTM Zone 39U is the coordinate system (in meters).

uplifted blocks of an accretionary prism. The unconformity contacts previously mapped as thrust faults may thus be better interpreted as contacts between autochthonous layers and ejected megablocks. Still, constraints are missing to unveil the extent and geometry of this impact structure. Caution should be taken when considering the drawn organization and orientation of the numerous slumped and/or uplifted blocks of the brecciated and shocked rocks represented beneath the Pliocene filling in the cross sections of Fig. 2, and particularly at depths greater than that of the drill holes. One should also keep in mind that the outcrops are rare, which argues in favor of the use of geophysical methods to investigate this area.

DATA AND METHODS

In September 2019, a field campaign was conducted to acquire ground magnetic and gravity field data and to collect samples for further petrophysical analyses. The villages, the forest, and the density of cultivated fields guided the choice of measuring potential-field data mainly along asphalted and dirt roads with an irregular grid showing more spatial resolution nearby the expected center of the structure (Fig. 3). The estimated size of the structure ($d \sim 10$ km) led us to acquire data up to about 17 km from this center, along at least two perpendicular directions. A total of 146 gravity and 6216 magnetic field data were acquired in 8 days, and 88 samples of impact fine-grained melt-bearing breccia and brecciated/fractured limestones were collected at eight sites mainly within the central and eastern quarries. Shatter cones were found in place at several sites (Fig. 3) within the allochthonous breccia, up to a distance of 4 km southeast from the central quarry (see Fig. S1 of the supporting information for details about this specific outcrop).

Ground Magnetic Field Survey

The magnetic field measurements were acquired using three MMPOS-1 scalar Overhauser magnetometers (two mobile and one fixed for base station measurements). The sampling rate was 30 s, and each measurement was georeferenced in (X,Y) by DLPOS GPS devices mounted on each set. The lateral precision of these GPS, between 2 m in clear area and 5 m in the forest, was sufficient to obtain a robust magnetic field map of the Karla impact structure. The height of the magnetic field probe was 2 m. The mean geomagnetic field intensity in the studied area during

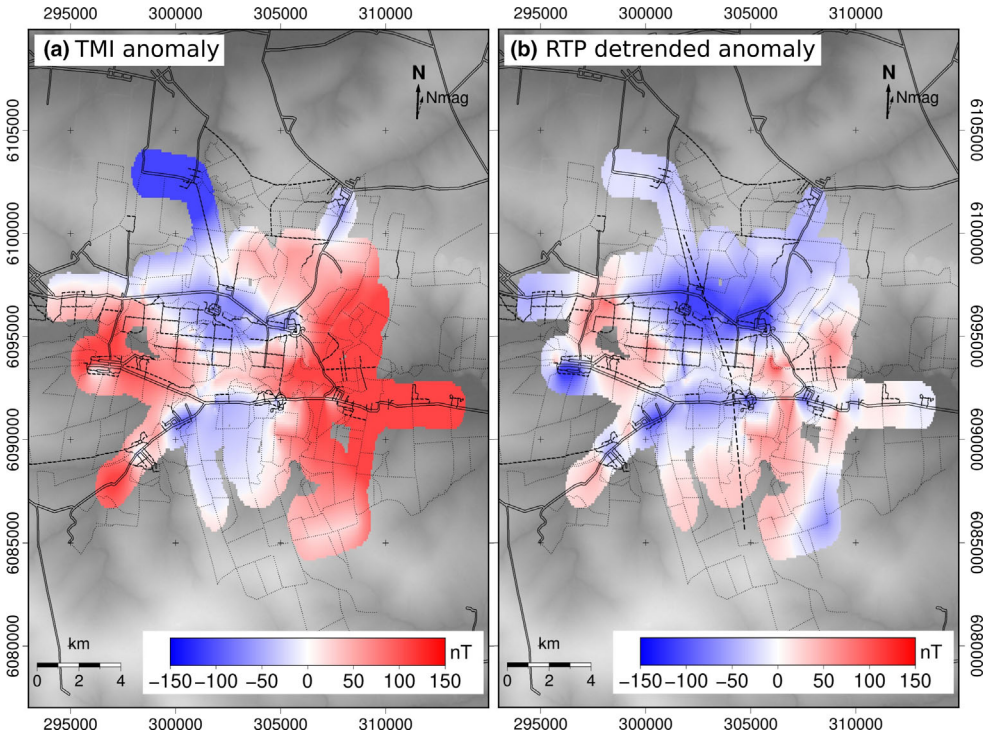

Fig. 4. Interpolated total magnetic intensity (TMI) (a) and detrended reduced-to-the-pole (RTP) (b) ground magnetic field anomaly maps over the Karla impact structure. In (b), the dashed line corresponds to the selected N-S profile for 2-D modeling (see Fig. 6).

our survey was 54,130 nT, while the IGRF-12 model predicted 53,980 nT (Thébault et al., 2015). The data from the mobile magnetometers were corrected from the weak (±10 nT) diurnal variations of the external magnetic field using observations from the static magnetometer. All outliers (mostly all data acquired within villages) were removed from the data set after a careful checking of each prospection line and the application of a time domain nonconvolution low-pass filter. A minimum curvature interpolation was then performed before the application of a degree 2 polynomial detrending surface to the interpolated grid (Fig. 4a). This allowed the removal of the regional magnetic crustal signal, which is apparently weak in the area, considering a contour magnetic field map in the leaflet associated with the geological map (Semakin et al., 1999). Eventually, we reduced the gridded data set to the pole (RTP, Fig. 4b), the geomagnetic field inclination and declination values being 72° and 13°, respectively.

Gravity Data Survey

Gravity field observations were acquired by using two mobile Scintrex CG-5 Autograv gravity meters with a 1 Hz sampling rate and by considering four or five successive cycles of measurements for 90 s at each site. After exclusion of possible outliers, the mean value of these four or five measurements was considered. Using the standard deviation on the mean, we obtained a mean value of 6 μGal for the instrumental error on sites, while the gravimeter drift varied between 1 and 2 μGal mn^{-1}. This drift was corrected by a return to the base every 3–4 h. The exact (X, Y, Z) coordinates of the gravity meter at each site were determined by using two differential Global Navigation Satellite System (GNSS) devices. In detail, two Trimble R10 mobile antennas were used to follow each gravity meter, which worked in parallel but at different sites, and were linked to a single common Trimble R9 GNSS base station by a standard radio communication. The real-time kinematics ability of the whole system allows achieving 5 and 10 cm of lateral and vertical precisions, respectively. These elevation data and all standard corrections were used to remove the influence of Earth tides, drift, latitude, altitude, and local topography (GEOINT, 2008). The EGM96 geoid was used as the altitude reference. The resulting complete Bouguer anomaly values were then obtained using 2100 kg m^{-3} as reference density (after several tests with different densities from 1800 to 2700 kg m^{-3}; see Fig. S2

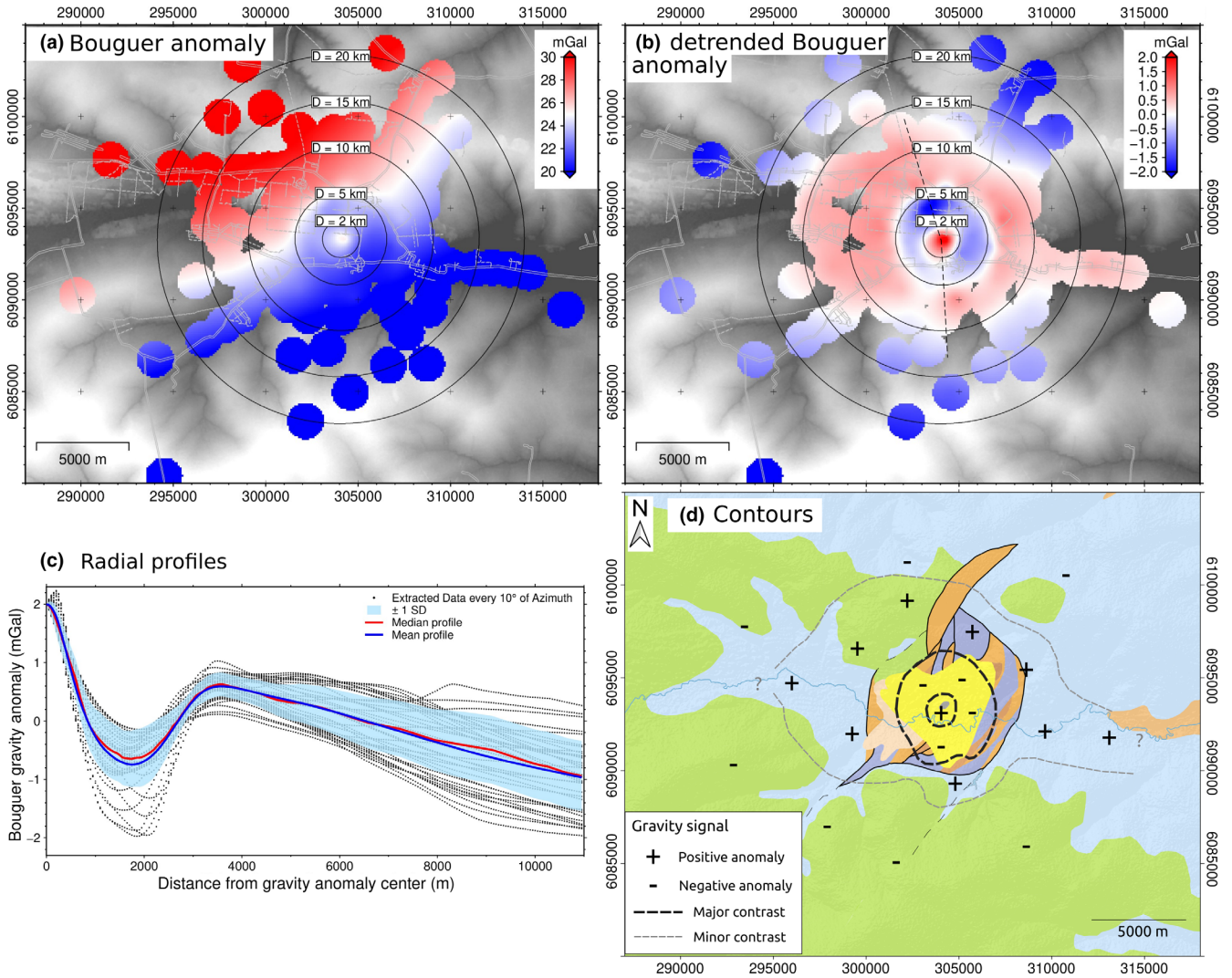

Fig. 5. Bouguer gravity anomaly map (a) before and (b) after detrending, with (c) radial profiles extracted from the residual Bouguer anomaly every 10° of azimuth (dashed lines) plus the median (red) and mean (blue) profiles and the ±1 sigma area (light blue), and (d) main contours of the residual Bouguer anomaly plotted over the geological map (see Fig. 2 for details). In (b), the dashed line corresponds to the selected N-S profile for 2-D modeling (see Fig. 6). For (a) and (b), the solid circles show different diameters *D*, while the grayscaled background corresponds to the SRTM digital elevation model of Fig. 1.

in the supporting information), with 0.03 mGal of accuracy. The leaflet associated with the geological map of Semakin et al. (1999) shows a very synthetic gravity anomaly regional map, revealing that the Karla impact structure is located in a Bouguer anomaly of 10–30 mGal (i.e., 20 mGal of amplitude), without any information about the detailed gradient at the scale of the gravity network measured. The global map of the WGM2012 model (Bonvalot et al., 2012) was considered for evaluating the regional signal: the Karla impact structure is located within an area of 15–20 mGal amplitude with a NW-SE regional decrease of −1 mGal km^{-1}. Extracting a degree 2 polynomial surface on the final interpolated grid shows a similar gradient. A fitted degree 2 polynomial surface was thus removed from our gravity data set as the regional trend (Figs. 5a and 5b).

Petrophysical Analyses on Samples

The petrophysical properties of the samples collected from the different lithologies encountered in the Karla impact structure were determined in the laboratory. A Quantachrome Helium stereopycnometer was used to measure the grain density. Porosity was further determined by measuring the volume of sample with standard shape using a caliper. Bulk “dry” densities were then calculated

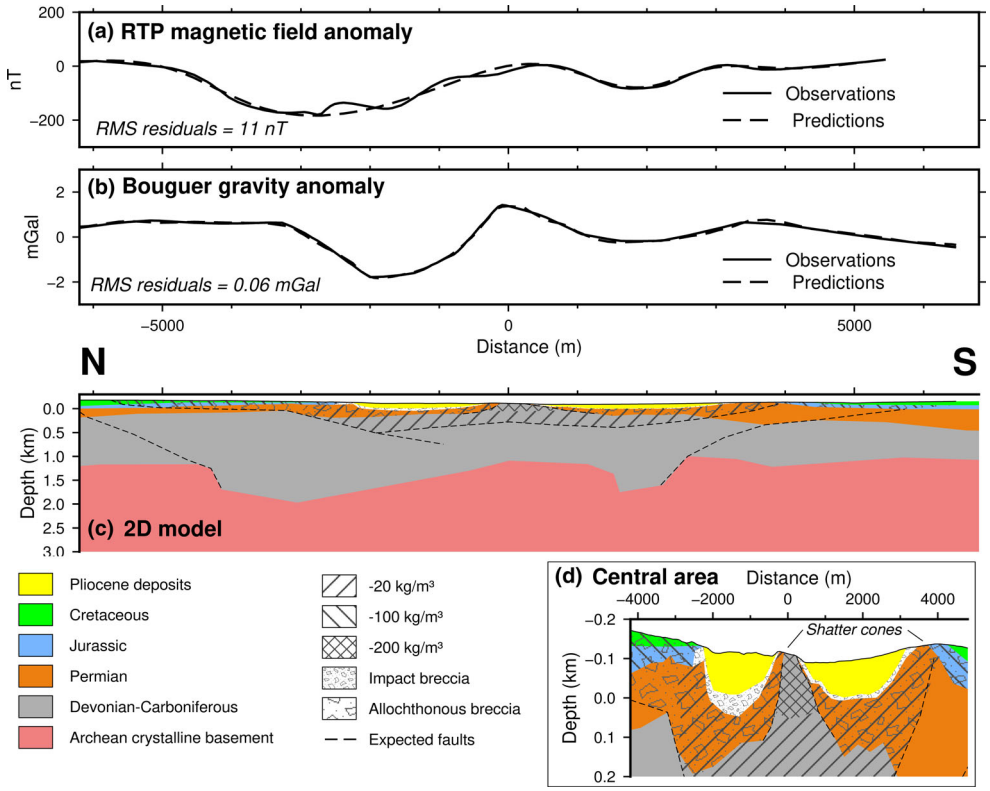

Fig. 6. 2-D model of the Karla impact structure constrained by potential-field data, petrophysical measurements on samples (Table 1), as well as previous geological constraints (drill holes and surface geology). The RTP magnetic field and Bouguer gravimetric anomaly observations and predictions along the selected profile (see Figs. 4 and 5) are shown in (a) and (b), respectively. The 2-D forward model is shown in (c) with no vertical exaggeration, whereas (d) zooms in the central area with a vertical exaggeration of 10. The *x*-axis of distance is expressed in meters from the expected center of the structure, in the main quarry.

using the mass of each sample. Magnetic properties were measured using an AGICO MFK1 Kappabridge for magnetic susceptibility, and a Superconducting Quantum Interference Devices (SQUID) 760R (2G Enterprises) for magnetic remanence. We did not get access to the samples of the drill holes shown in Fig. 2.

Modeling

These three sets of data, plus previous geological information (maps, cross sections, and synthetic logs of the drill holes), were used as inputs for building 2-D forward models of the impact structure, using the GM-SYS module of the GEOSOFT Oasis montaj software delivered by SEEQUENT.

RESULTS

Magnetic Field Anomaly

Figure 4 displays the magnetic field maps over the Karla impact structure. The total magnetic intensity anomaly map shows that significant signals up to 300 nT of anomaly amplitude were observed in the area, although the surface geological formations (clays and limestones) should be weakly magnetized. The RTP map reveals a complex anomaly shape with a general negative (about −100 nT) anomaly, along the roads north and south of the Karla river (after deleting all noisy data acquired in villages). On the contrary, the western and eastern parts show positive anomalies, while the expected geographic center is located in a subnull anomaly area with about −25 nT nearby the central quarries. Compared to the geological map, the generally negative anomaly area corresponds marginally to the brecciated/fractured rocks and the Pliocene deposits.

Bouguer Gravity Anomaly

The residual Bouguer gravity anomaly map is shown in Fig. 5b. On average, a clear radially symmetric structure centered on the crater center is observed. The center (quarry area; diameter ~2 km)

Table 1. Petrophysical properties[a] of the lithologies of the Karla impact structure.

Lithologies	Density (kg m^{-3})	Magnetic susceptibility (10^{-3} SI)	Natural remanent magnetization (10^{-3} A m^{-1})
Neogene deposits (clays, siltstones)	2130	–	–
Impact breccia[b]	1700–1900	−0.004 to 0.006	0.007–0.046
Cretaceous clays	2200	–	–
Jurassic clays and marls	2200–2300	–	–
Permian clays, siltstones, and marls	2360–2380	–	–
Devonian/Carboniferous limestones[b]	2330–2660	−0.01 to 0.004	0.003–0.012
Archean crystalline basement	2650	50	–

[a]Ranges of values correspond to the minimum and maximum values in the best-fitting forward model of Fig. 6.
[b]Sampled lithologies with experimental data. Other density data are typical values for the same type of rocks from Carmichael (1989).

corresponds to a positive Bouguer anomaly of +2 mGal, surrounded by a 1.5 km wide ring of about −0.2 to −1.5 mGal anomaly, which broadly correlates with the Pliocene deposits. From 2.5 to about 5–7 km of radial distance, the Bouguer anomaly becomes positive up to about +0.5 mGal, and then decreases monotonically on average (Fig. 5c), reaching -1 ± 0.5 mGal at about 10 km of radial distance. Only in the eastward direction along the main road toward Buinsk town in the Karla river valley, the signal remains positive (Fig. 5d). The latter may be associated with the incision of Jurassic and Cretaceous deposits in this direction of the valley (i.e., regional geology, not influenced by the impact). The gravity anomaly radial profiles every 10° of azimuth (Fig. 5c) show that the described trends are coherent irrespective of the direction, the standard deviation ranging from 0.2 to 1 mGal. However, it also reveals that outside the negative ring, the signal constantly decreases from about +1 mGal to −1 mGal, without observing any flattening of this decrease even at a radial distance larger than 10 km, despite the anisotropic behavior of this decrease (i.e., larger standard deviation of the profiles).

MODELING RESULTS

The observation of concentric Bouguer anomalies is consistent with the presence of rocks impacted by an extraterrestrial body, but the succession of positive and negative anomalies should be further investigated by modeling the geological and geometrical properties of the Karla impact structure. A N-S profile (Figs. 4b and 5b) was considered for this 2-D forward model (Fig. 6), which is constrained by petrophysical measurements on the collected samples (Table 1). The impact breccia is the least dense formation, because of its high porosity. We also attribute a low density to the poorly consolidated Neogene deposits. Some blocks of Carboniferous limestones possess densities of about 2330 kg m^{-3} in the main quarry, and 2660 kg m^{-3} in the eastern quarry. Both the impact breccia and these limestone rocks have very weak induced and remanent magnetization intensities. Only the Archean crystalline basement (not sampled) must possess a significant magnetization (magnetic susceptibility of 0.05 SI).

These parameters were then used as initial parameters in the 2-D model, which also considers the information from the drill holes and the surface geology. After several iterations by using slight reduction of the density properties (e.g., from 2300 to 2200 kg m^{-3} for some parts of the Mesozoic formations) nearby or within the Karla impact structure (due to brecciation and/or fracturing) and/or by adjusting the geometry of the lithological units, a best-fitting model was found along the N-S selected profile (Fig. 6; see also Fig. S3 of the supporting information for a more detailed version of the model).

The root-mean square misfits are 11 nT and 0.06 mGal for the magnetic and gravity signals, respectively. The resulting model is different than the geological cross sections of Fig. 2. The main difference is the basement uplift up to about 1 km of depth, which is necessary to explain the observed magnetic anomalies in the area because all post-Archean geological formations have very low magnetization. The central positive gravimetric anomaly is partly explained by this basement uplift and by the one of the Paleozoic formations. Besides, these layers may be affected by faulting and/or folding at about 1 km depth. A significant reduction in rock density of −200 kg m^{-3} is observed in the top of the central uplift, indicating highly shocked rocks (which fits with the shatter cone occurrences in this area). The ring of negative gravity anomaly is partially due to the postimpact Pliocene filling lacustrine sediments, and by the presence of the impact breccia layer with a very low density (1700–1900 kg m^{-3}). The rock densities are also slightly reduced by 20–100 kg m^{-3} in a central zone of 7 km of diameter and 400–500 m of thickness. It corresponds to the allochthonous breccia (Masaitis, 1999) which were fractured/brecciated during the compression stage of the impact, reducing their density, but some samples reveal that it was cemented, filling fractures and

pores. Actually, we could also attribute these low density areas to the collapsed disruption cavity (and the slump block zone) surrounding the central uplift (Hildebrand et al., 1998; Pilkington & Hildebrand, 2003). The shallow Mesozoic formations with a reduced density of -100 kg m^{-3} up to 6 km of radial distance from the center probably correspond to the same fracturing/brecciation process as within allochthonous breccia, but these formations were not affected by cementation. However, a positive Bouguer anomaly signal is observed to the north and is caused either by the Devonian-Carboniferous limestone formation (here at 2660 kg m^{-3}) and/or by the relatively shallow (only ~1.2 km of depth) Archean basement. The positive magnetic field anomaly argues in favor of a small uplift of this crystalline basement.

DISCUSSION

Our geophysical measurements clearly confirm the anomalous geological subsurface composition in the area of the Karla impact structure, and help to image the geometry of the affected formations. They unveil several issues about its size and its age.

Gravity Anomaly and Size

Mainly two "diameters" can be determined for an impact structure: the diameter (D) of the pristine crater, which is defined morphologically by the rim crest; and the apparent crater diameter (D_a), which is mainly used for most of the terrestrial craters (i.e., eroded to some degree). D_a is usually defined by concentric normal faults or the crater rim monocline, or by the extent of a circular geophysical anomaly (Kenkmann et al., 2014; Osinski & Ferrière, 2016). On Earth, erosion, sedimentation, and tectonics have usually obliterated or reduced the morphological signature of impact crater rims. In addition, rock exposure conditions and postimpact sedimentary filling of the crater hinder easy determination of D and D_a. Usually, a circular negative gravimetric anomaly can be observed over impact structures, and its diameter approximately reflects D (Pilkington & Grieve, 1992), but it clearly depends on the amount of erosion and could be considered a minimum diameter. However, the "ringlike" shape of alternating positive and negative Bouguer gravity anomalies in Karla is not so typical of complex impact structures with $D < 20$ km.

Comparison with Bouguer Signatures of Other Impact Structures

To our knowledge, similar patterns have been only described for the <34 Ma Jebel Waqf as Suwwan (Jordan), 56–145 Ma Connolly Basin (Western Australia, WA), and 86 Ma Yallalie (WA) impact structures (Fig. 7) (Hawke, 2004; Heinrichs et al., 2014; Shoemaker et al., 1989). They all possess a diameter between 5 and 12 km, and their targets are sedimentary. The gravity data acquired over Jebel Waqf as Suwwan show an intense 2 km wide central residual Bouguer anomaly of +4 mGal, a narrow -0.5 to -1 mGal ring, a 1 km wide +0.3 mGal ring, and another -0.1 mGal anomaly ring, from center to the rim (Heinrichs et al., 2014). The associated forward model explains these rings by the presence of a 400 m amplitude "syncline-like" topography of an important interface between two layers (gray and white layers in Fig. 7b) with a 515 kg m^{-3} density contrast, whereas the high central peak is caused by the quasi-outcropping of the dense Paleozoic uplifted layers (mainly sandstones, in white in Fig. 7b) (Kenkmann et al., 2017). Jebel Waqf as Suwwan is better preserved than Karla, still showing a 30–50 m amplitude circular topography remaining from a 6 km wide outer ring and 1 km wide central uplift, while the erosion was estimated to be about 500 m. Gravity investigations over the 9 km diameter Connolly Basin impact structure also revealed a +3 mGal central gravity anomaly of about 3–4 km of wavelength, surrounded by thinner rings of -1 mGal and +0.5 mGal anomalies (Hawke, 2004; Shoemaker et al., 1989). A central uplift of Permian dense formations, partially seen in the seismic data, may explain this central positive peak, while the rings may correspond to the signals due to a thinner shallow breccia layer and an overlying crater filling deposit. The +0.5 mGal signal surrounding the narrow gravity low is due to high density sediments shed off the central peak in the annular low. Again, despite its older age, the Connolly Basin still displays a rim 20–30 m higher in elevation than the central part of the structure. Interestingly, the Yallalie impact structure shows an 8 mGal amplitude positive central gravity anomaly with about 20 km of wavelength, surrounded by weaker positive anomalies of +2 or +3 mGal. The total extent of these gravity anomalies reaches about 40 km, while the crater rim diameter was estimated to be 12 km only (Hawke, 2004). Clearly this diameter should be revised, and if we consider $D = 40$ km, the overall signal mimics—at larger scale—the one observed at Karla for $D = 10$ km.

Implications on the Deep Structure of Karla, and Its Size

The central uplift in Karla is expressed in the gravity data by the central positive anomaly located over the main quarry, surrounded by a negative anomaly ring, which may a priori correspond to the collapsed disruption zone and/or with the trough filled by allochthonous and impact breccia and by postimpact Pliocene lacustrine sediments. Similar Pliocene filling

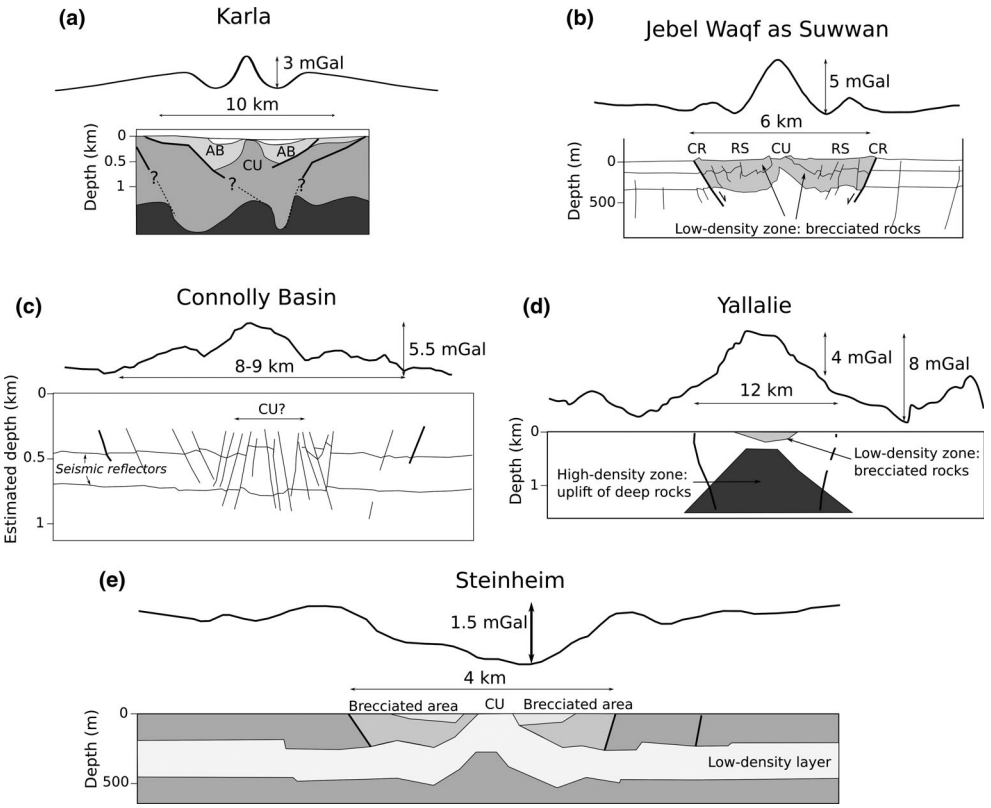

Fig. 7. Comparison between the Bouguer gravity anomaly (top) and associated models (bottom) for Karla (a; this study), Jebel Waqf as Suwwan (b), Connolly Basin (c), Yallalie (d), and Steinheim (e) impact structures. The Karla profile and model (a) correspond to a simplified version of Fig. 6. All other profiles and models were modified from Heinrichs et al. (2014) and Kenkmann et al. (2017) for (b), Hawke (2004) for (c) and (d), and from Ernstson (1984) for (e). The main faults representing the expected crater rim are represented by thick lines. All crater models but Karla benefited from seismic data. AB = allochthonous breccia; CU = central uplift; CR = crater rim; RS = ring syncline.

with a central lake has been described for Yallalie, but this does not seem to decrease the central gravity high (Fig. 7d). On average, the gravimetric signature and the associated models of the Karla impact structure are similar to the ones of Jebel Waqf as Suwwan and Connolly Basin. In particular, the faults identified by seismic data beneath the crater rim of those two craters, and also partly exposed for Jebel Waqf as Suwwan (Heinrichs et al., 2014; Kenkmann et al., 2017), seem to correspond with the end of the gravity anomaly (Figs. 7b and 7c). Therefore, we can assume that the faults (or geological contacts) delimiting the allochthonous breccia of the Karla impact structure may also indicate the crater rim: it leads to about 6–8 km of diameter. Outside this expected crater rim, the signal constantly decreases, at least up to about 12–13 km of radial distance (Fig. 5). This behavior is enigmatic and leads us to admit that we cannot conclude the maximum size of the gravity anomaly due to the impact. Perhaps the still positive Bouguer anomaly in the Karla river valley eastward, which disagrees with the constant decrease observed elsewhere, may indicate the influence of the regional signal (here positive because of the incision of Cretaceous and Jurassic strata which lets the denser Permian formations outcropping). However, the constant decrease from 3–4 km of radial distance to 12–13 km may also correspond to the regional crustal signal. Finally, one can use empirical relationships to estimate the diameter of Karla. For instance, the ~1 km height of the central uplift is consistent with a ~10 km diameter crater according to Grieve et al. (1981; see also Grieve & Therriault, 2004). Considering the ~2 km width (D_{CU}) of this uplift and $D_{CU} = 0.2–0.25\ D$ (Pike, 1985), then we obtain a range between 8 and 10 km for the diameter of Karla. The size of this central uplift also constrains the diameter of the collapsed disruption zone (D_{CDC}) to about 4–5 km, which is consistent with the diameter of the ring showing a gravity low. Using $D_{CDC} = 0.49\ D$ (Pilkington & Hildebrand, 2003), we

also find a diameter between 8 and 10 km for the complex Karla impact structure. Thus, a range between 8 and 10 km for D can be suggested, based on the gravity anomaly analysis. An analog would then be the Steinheim impact structure, with a relatively similar Miocene (15 Ma) age and a sedimentary target (Buchner & Schmieder, 2015). With a diameter D of 3.8 km (Kenkmann, 2021), smaller than the expected one for Karla, its Bouguer gravity signature corresponds to a 1.5 mGal negative anomaly observed over a diameter of about 6–7 km (Fig. 7e) (Ernstson, 1984), while the diameter of the crater cavity was first estimated based on the present-day depression of 3–4 km. Interestingly, the Karla and Steinheim impact structures do not show any evidence of impact ejecta. This may be due to the erosion of this ejecta layer because of the regional elevated position of this impact crater. Nevertheless, this weak negative signal is here due to the uplift of a low density stratigraphical layer (shown in white in Fig. 7e) (Ernstson, 1984). Thus, Steinheim, despite having an apparent similar structure like Jebel Waqf as Suwwan and Karla, shows a resulting opposite gravity anomaly, which represents the standard low signal observed over small size craters of sedimentary target. Still, again, the gravity anomaly is larger than the apparent diameter. Therefore, even a gravity anomaly of about 12 km in maximum size for Karla may mean a lower apparent diameter of about 8–10 km. Another argument in favor of this diameter is the size of the most significant ground magnetic field anomalies observed in Karla, which extends over an area of ~10 km too, while the drill holes outside this 10 km diameter did not reveal any brecciated/fractured formation, to our knowledge.

Implications on Age and Erosion

A Post-Cretaceous Probably Late Miocene Age for Karla

After careful revision of Masaitis et al. (1976, 1980), it appears that the age of the Karla impact structure cannot be better determined than between ~66 Ma and ~4 Ma based on stratigraphy alone, even if the Pliocene age of the lacustrine sediments filling the annular trough suggests an age close to this ~4 Ma bound. Our results confirm the occurrence of an impact in the area (geophysical anomalies and new shatter cone findings in the central uplift and the allochthonous breccia), but we do not provide new stratigraphic constraint on the age of the impact event. Nevertheless, the 2-D model derived from the geophysical data shows that Permian rocks plus the Jurassic and Cretaceous strata are shocked/fractured within and nearby the allochthonous breccia and Pliocene clay deposits at the center. Paleogene rocks are totally missing in the regional stratigraphy. Therefore, our model agrees with a post-Cretaceous age for the impact, but we cannot be more specific. All other information on the age derive from the material, now unfortunately inaccessible, recovered in the drill holes.

Erosion Rate

If we consider Karla a "young" impact, with an age less than 30 Ma, then its present-day morphological signature should be a little more significant, resembling those of Jebel Waqf as Suwwan and/or Connolly Basin, except if the erosion rate in this area was larger than elsewhere. Of course, the latter two impact structures are located in arid climate areas, while Karla underwent a cold climate in the Russian plains of the East European platform since at least the early Miocene, even if it was not glaciated during the Pleistocene (Hergarten & Kenkmann, 2019; Willenbring & Jerolmack, 2015; Willenbring & von Blanckenburg, 2010). Relatively low erosion rates of about 10–20 m Ma^{-1} can be considered for such cold regions (Harel et al., 2016; von Blackenburg, 2005), meaning that the topography over the Karla impact structure may have lost 100–600 m at most. The postimpact sedimentary filling may have thus been 100–600 m thicker than the present-day 100 m-thick deposit. In this case, it may have filled a wider area, perhaps overlying the fractured Jurassic and Cretaceous rocks up to 5 km of radial distance. Nevertheless, the 10–20 m Ma^{-1} regional erosion rate is a minimum value to be considered, since the Karla impact crater was the only morphological anomaly in this area of the flat East European Platform 10 Myr ago. For impact craters on marl and limestone targets, the crater topography is also generally smoother than the one on crystalline targets (Osinski & Pierazzo, 2013), so a cavity of about 200 m height can be expected for Karla. Still the rim of a crater is the most favorable topography to be eroded, while the central sedimentary filling (in a postimpact lake) also played a role to smooth the crater topography. According to Ernstson (1984), the postimpact erosion and filling of the Steinheim impact structure seems to have erased a 500–600 m deep initial excavation, which clearly shows that an impact crater may lose its morphology in 10–15 Ma. However, the sequence of allochthonous breccia in the ring syncline covered by lake deposits indicates that only 50–100 m of erosion is expected within the Steinheim crater interior. Therefore, these uncertainties clearly show that, for a relatively young and buried impact structure like Karla, more investigations are needed, perhaps outside the impact structure, in order to better estimate the regional erosion of the sediments

of the East European platform. Nevertheless, after careful considerations about the expected topography, the postimpact erosion, and the comparison with other young structures, it seems that an impact event older than 10 Ma is not mandatory for explaining the present-day appearance of the Karla impact structure, arguing in favor of the initial age estimations (Masaitis, 1999).

Magnetized Source

In our model, the magnetic field anomalies observed over the Karla impact structure are explained by the magnetization contrasts implied by the uplift of the crystalline basement. Indeed no intense magnetization is associated with the post-Archean sedimentary formations. Within the core of the central uplift of the Haughton crater with a similar carbonate target, we observed that the postimpact hydrothermal alteration had significantly increased the magnetization almost up to the present-day surface (Quesnel et al., 2013; Zylberman et al., 2017). However, the long wavelengths of the magnetic field anomalies observed in Karla exclude a shallow (<1 km depth) source. Still Hawke (2004) reported that the faulting in crater areas favored the occurrence of significant hydrothermal alteration cells, which led to local postimpact remagnetization creating magnetic field anomalies. Our magnetic field measurements over the Karla structure do not support such intense remagnetization due to the lack of a significant amount of ferromagnetic minerals and remanent magnetization (Table 1) in the Paleozoic and Mesozoic rocks, as well as in the impact breccia, but we cannot exclude such magnetization processes in the uplifted part (at ~1 km depth) of the Archean basement. Besides, such hydrothermal fluid circulation may also explain the cementation of the allochthonous breccia: quartz and chalcedony seem to dominate the mineralogical composition of the cement. Further petrographical investigations on samples are needed to better characterize the amplitude and duration of this possible postimpact hydrothermal alteration in Karla.

CONCLUSIONS

The Karla impact structure has been little studied to date, with only brief mentions in review publications about Russian craters, and a geological description based on rare outcrops and regional drill holes, which were mostly analyzed in a tectonic interpretative framework until the short descriptions by Masaitis et al. (1980). Our study is the first to focus on the geological structure of Karla via potential-field observations. Using ground measurements, we unveil significant gravity and magnetic field anomalies, which constrain the structure of the remains of the impact crater. The Bouguer gravity signal shows a positive central peak of +2 mGal (due to the Archaean basement and Paleozoic layer uplift) compared to a ring of negative −1 mGal anomaly up to 6 km of diameter. A circular positive anomaly is then observed, which decreases up to 20 km of diameter at least. Such a gravity signature can only be compared to those observed over Jebel Waqf as Suwwan, Connolly Basin, and (at larger scale) Yallalie impact structures, of similar size and sedimentary target. The geophysical models associated with these craters suggest that the remains of the Karla crater rim are delimited by the main contacts (faults?) between allochthonous breccia and the surrounding Mesozoic formations. This suggests a diameter between 8 and 10 km. The ground magnetic field anomalies are significant (amplitude up to 200 nT) and seem also restricted in a 10 km diameter area. Our modeling results show that the crystalline basement uplift implies strong magnetization contrasts, which lead to such magnetic field anomalies. Last, this model agrees with the smoothing of the crater morphology by erosion and/or by sedimentary filling, in about 10–30 Ma.

Acknowledgments—This work was supported by the Russian Foundation for Basic Research (RFBR grant no.18-55-15014) and by CNRS PRC French program. This study was a partial contribution to the research theme of the Vernadsky Institute of Geochemistry and Analytical Chemistry RAS. The gravity meters were kindly provided by the Institute of Geology and Petroleum Technologies, of the Kazan Federal University (KFU), and the RTK GPS devices by the Department of Astronomy and Space Geodesy, KFU. We gratefully acknowledge the reviewers, A. Hildebrand, T. Kenkmann, and Y. Marangoni, and the associate editor, J. Plescia, for their precious comments and suggestions, which greatly improved the quality of the manuscript.

Data Availability Statement—The data used in this study can be downloaded here: https://doi.org/10.34930/1210822c-ffc1-4b75-9234-169d7baf89c9.

Editorial Handling—Dr. Jeffrey Plescia

REFERENCES

Bonvalot, S., Balmino, G., Briais, A., Kuhn, M., Peyrefitte, A., Vales, N., Biancale, R., Gabalda, G., Reinquin, F., and Sarrailh, M. 2012. *World Gravity Map. Commission for the Geological Map of the World.* Paris: BGI-CGMW-CNES-IRD.

Buchner, E., and Schmieder, M. 2015. The Steinheim Basin Impact Crater (SW-Germany)—Where Are the Ejecta? *Icarus* 250: 529–43. https://doi.org/10.1016/j.icarus.2014.12.026.

Carmichael, R. S. 1989. *Practical Handbook of Physical Properties of Rocks and Minerals*, 354. Boca Raton, FL: CRC Press.

Ernstson, K. 1984. A Gravity-Derived Model for the Steinheim Impact Crater. *Geologische Rundschau* 73: 483–98. https://doi.org/10.1007/BF01824969.

GEOINT. 2008. Gravity Station Data Format & Anomaly Computations. Washington, D.C.: National Geospatial-Intelligence Agency of the USA.

Gottwald, M., Kenkmann, T., and Reimold, U. 2020. *Terrestrial Impact Structures: The Tan-DEM-X Atlas*. Munich: Pfeil-Verlag.

Gradstein, F. M., Ogg, J. G., Schmitz, M. D., and Ogg, G. M. 2020. *Geologic Time Scale 2020*. Amsterdam: Elsevier.

Grieve, R. A. F., Robertson, P. B., and Dence, M. R. 1981. Constraints on the Formation of Ring Impact Structures, Based on Terrestrial Data, in Multi-Ring Basins. In *Proceedings, 12th Lunar and Planetary Science Conference*. pp. 37–57.

Grieve, R. A. F., and Therriault, A. M. 2004. Observations at Terrestrial Impact Structures: Their Utility in Constraining Crater Formation. *Meteoritics & Planetary Science* 39: 199–216. https://doi.org/10.1111/j.1945-5100.2004.tb0036.x.

Harel, M.-A., Mudd, S. M., and Attal, M. 2016. Global Analysis of the Stream Power Law Parameters Based on Worldwide 10Be Denudation Rates. *Geomorphology* 268: 184–96. https://doi.org/10.1016/j.geomorph.2016.05.035.

Hawke, P. J. 2004. *The Geophysical Signatures and Exploration Potential of Australia's Meteorite Impact Structures*, 343. PhD thesis, University of Western Australia, Perth, Australia.

Heinrichs, T., Salameh, E., and Khouri, H. 2014. The Waqf as Suwwan Crater, Eastern Desert of Jordan: Aspects of the Deep Structure of an Oblique Impact from Reflection Seismic and Gravity Data. *International Journal of Earth Sciences* 103: 233–52. https://doi.org/10.1007/s00531-013-0930-4.

Hergarten, S., and Kenkmann, T. 2019. Long-Term Erosion Rates as a Function of Climate Derived from the Impact Crater Inventory. *Earth Surface Dynamics* 7: 459–73. https://doi.org/10.5194/esurf-7-459-2019.

Hildebrand, A. R., Pilkington, M., Ortiz-Alemean, C., Chavez, R. E., Urrutia-Fucugauchi, J., Connors, M., Graniel-Castro, E., Camara-Zi, A., Halpenny, J. F., and Niehaus, D. 1998. Mapping Chicxulub Crater Structure with Gravity and Seismic Reflection Data. In *Meteorites: Flux with Time and Impact Effects*, edited by M. M. Grady, R. Hutchison, G. J. H. McCall, and D. A. Rothery. Geological Society London, Special Publications 140, 155–76.

Kenkmann, T. 2021. The Terrestrial Impact Crater Record: A Statistical Analysis of Morphologies, Structures, Ages, Lithologies, and More. *Meteoritics & Planetary Science* 56: 1024–70. https://doi.org/10.1111/maps.13657.

Kenkmann, T., Poelchau, M., and Wulf, G. 2014. Structural Geology of Impact Craters. *Journal of Structural Geology* 62: 156–82. https://doi.org/10.1016/j.jsg.2014.01.015.

Kenkmann, T., Sturm, S., Krüger, T., Salameh, E., Al-Raggad, M., and Konsul, K. 2017. The Structural Inventory of a Small Complex Impact Crater: Jebel Waqf as Suwwan, Jordan. *Meteoritics & Planetary Science* 52: 1351–70. https://doi.org/10.1111/maps.12823.

Masaitis, V. L. 1999. Impact Structures of Northeastern Eurasia: The Territories of Russia and Adjacent Countries. *Meteoritics & Planetary Science* 34: 691–711. https://doi.org/10.1111/j.1945-5100.1999.tb01381.x.

Masaitis, V. L., Danilin, A. N., Karpov, G. M., and Raikhlin, A. I. 1976. Karla, Obolon, Rotmistrovka Astroblemes in European Part of the USSR. *Doklady ANSSSR* 230: 174–7 (in Russian).

Masaitis, V. L., Danilin, V. N., Mashchak, M. S., Raikhlin, A. I., Selivanovskaya, T. V., and Shadenkov, E. M. 1980. *The Geology of Astroblemes*, 231. Leningrad, Russia: Nedra Press.

Osinski, G. R., and Ferrière, L. 2016. Shatter Cones: (Mis) Understood? *Science Advances* 2: e1600616. https://doi.org/10.1126/sciadv.1600616.

Osinski, G. R., and Pierazzo, E. 2013. *Impact Cratering: Processes and Products*, 330. Chichester: Wiley-Blackwell.

Pike, R. J. 1985. Some Morphologic Systematics of Complex Impact Structures. *Meteoritics* 20: 49–68.

Pilkington, M., and Grieve, R. A. F. 1992. The Geophysical Signature of Terrestrial Impact Craters. *Reviews of Geophysics* 30: 161–81. https://doi.org/10.1029/92RG00192.

Pilkington, M., and Hildebrand, A. R. 2003. Transient and Disruption Cavity Dimensions of Complex Terrestrial Impact Structures Derived from Magnetic Data. *Geophysical Research Letters* 30: 2087. https://doi.org/10.1029/2003GL018294.

Popov, S. V., Shcherba, I. G., Ilyina, L. B., Nevesskaya, L. A., Paramonova, N. P., Khondkarian, S. O., and Magyar, I. 2006. Late Miocene to Pliocene Palaeogeography of the Parathethys and Its Relation to the Mediterranean. *Palaeogeography, Palaeoclimatology, Palaeoecology* 238: 91–106. https://doi.org/10.1016/j.palaeo.2006.03.020.

Quesnel, Y., Gattacceca, J., Osinski, G. R., and Rochette, P. 2013. Origin of the Central Magnetic Anomaly at the Haughton Impact Structure, Canada. *Earth and Planetary Science Letters* 367: 116–22. https://doi.org/10.1016/j.epsl.2013.02.032.

Semakin, Y. G., Grishina, S. N., Vinogradov, O. R., Rudnev, M. L., Podateleva, L. P., and Balunez, Z. B. 1999. The Explanatory Note to the State Geological Map, Scale 1:200000, the Srende Volzhskay Series, N-38-XII, N-39-VII (in Russian). Moscow. http://www.geolkarta.ru/list_200.php?idlist = N-38-XII&idlist_d = G&gen = 1&g = 1.

Shoemaker, E. M., Shoemaker, C. S., and Plescia, J. B. 1989. Gravity Investigation of the Connolly Basin Impact Structure, Western Australia (Abstract #1010). 20th Lunar and Planetary Science Conference. CD-ROM.

Thébault, E., Finlay, C., Beggan, C. D., Alken, P., Aubert, J., Barrois, O., Bertrand, F. et al. 2015. International Geomagnetic Reference Field: The 12th Generation. *Earth, Planets and Space* 67: 79. https://doi.org/10.1186/s40623-015-0228-9.

von Blackenburg, F. 2005. The Control Mechanisms of Erosion and Weathering at Basin Scale from Cosmogenic Nuclides in River Sediment. *Earth and Planetary Science Letters* 237: 462–79. https://doi.org/10.1016/j.epsl.2005.06.030.

Willenbring, J. K., and Jerolmack, D. J. 2015. The Null Hypothesis: Globally Steady Rates of Erosion, Weathering Fluxes and Shelf Sediment Accumulation During Late Cenozoic Mountain Uplift and Glaciation. *Terra Nova* 28: 11–8. https://doi.org/10.1111/ter.12185.

Willenbring, J. K., and von Blanckenburg, F. 2010. Long-Term Stability of Global Erosion Rates and Weathering During Late-Cenozoic Cooling. *Nature* 465: 211–4. https://doi.org/10.1038/nature09044.

Zylberman, W., Quesnel, Y., Rochette, P., Osinski, G., Marion, C., and Gattacceca, J. 2017. Hydrothermally-Enhanced Magnetization at the Center of the Haughton Impact Structure, Nunavut, Canada. *Meteoritics & Planetary Science* 52: 2147–65. https://doi.org/10.1111/maps.12917.

SUPPORTING INFORMATION

Additional supporting information may be found in the online version of this article.

Fig. S1. Details about the shatter cone outcropping 4.0 km towards SE from the center of the Karla impact structure with (a) location map, (b) view of the cliffs of site 1 from west, (c) zoom on the site 1 at the top of the cliff (D.B. for scale), (d) shatter cone found in place at site 2, (e) view from south of the small quarry of site 2, (f) view of the outcrop of site 2.

Fig. S2. Residual Bouguer anomaly map using different density reduction of 1800, 2000, 2400 and 2670 kg m^{-3} for (a), (b), (c) and (d), respectively (Figure 5 of the main manuscript uses 2100 kg m^{-3}). It shows that using 1800, 2000 or 2100 kg m^{-3} as density value for Bouguer reduction, a circular central anomaly is observed, while using a density of 2400 or 2670 kg m^{-3}, the topographical effect is still visible (positive E-W elongated anomaly in the direction of the Karla river valley with just a 'dipolar' central anomaly). Grayscaled background corresponds to the SRTM digital elevation model shown in Figure 1 of the main manuscript.

Fig. S3. Same model as shown in Figure 6 of the main manuscript with block labels of density (italics) and magnetic susceptibility (in brackets) values.